Molecular Modeling of Polycarbonate. 1. Force Field, Static Structure, and Mechanical Properties

Cun Feng Fan,* Tahir Çağın, and Zhuo Min Chen

Molecular Simulations, Inc., Pasadena Research Center, 199 South Los Robles Avenue, Suite 540, Pasadena, California 91101

Kennith A. Smith

Corporate Research and Development Center, General Electric Company, Schenectady, New York 12301

Received April 12, 1993; Revised Manuscript Received February 7, 1994®

ABSTRACT: Molecular simulations of Bisphenol A polycarbonate were performed using a modified version of the Dreiding force field. In general, the simplicity of this generic force field was maintained. However, a few parameters were optimized by using *ab initio* calculations in order to generate better backbone torsional potentials. The validity of this modified force field was tested on a model compound similar to polycarbonate, 4,4′-isopropylidenediphenylbis(phenyl carbonate). The crystallographic data obtained from simulations of the model compound agreed well with the experimental data. The modified force field was then used in simulations of the glassy polymer. Model amorphous structures of Bisphenol A polycarbonate were built and optimized using periodic boundary conditions. The structure factor, $S(k)$, was calculated from pair distribution functions of the model structures. The peak positions in calculated $S(k)$ compare well with those obtained experimentally. The effects of the initial density on chain packing were also studied. Its impacts on the final density and energy are described. A general approach for calculating the stiffness matrix of any shape unit cell (triclinic system) is presented. A yield phenomenon for the model system was observed at about 10% strain. This value is comparable with experimental results (6–8%). The yield stress (0.25 GPa), however, was higher than experimental values, as was the Young's modulus at small strain. These results could be partially explained by the fact that the calculated mechanical properties represent an ideal structure and thus provide the upper limit values for the polymer.

Introduction

Molecular modeling of Bisphenol A polycarbonate has stimulated much interest recently, partly because of its commercial importance as an engineering plastic and partly because of the characteristics of its chain structure. Much of the previous experimental and molecular modeling effort on polycarbonate is summarized in a series of recent papers.[1] Polycarbonate serves particularly well as a candidate for the modeling of amorphous polymers since it contains almost no crystalline domains in the glassy state. This homogeneity eliminates the complexity caused by the crystallinity normally occurring in other polymers such as polyethylene. The properties derived from simulated amorphous polycarbonate are therefore more likely to correspond to the macroscopic properties measured by experiment (even though the simulated structures are necessarily composed of a limited number of atoms). Polycarbonate is also a good model since it exhibits certain dynamic features of segmental motion such as flips of the phenylene ring which may be characteristic of polymers with similar moieties along their backbone. Molecular modeling (molecular mechanics and dynamics) may be expected to at least partially explain the atomistic basis of these interesting dynamic features. It is also possible that molecular simulations will reveal new phenomena.

A correct description of the interactions between atoms, *i.e.*, a good force field, is essential in ensuring that simulation results are meaningful and reliable. In general, the process of obtaining accurate force field parameters can be very complex. In addition to experimental structural and spectral data, many high-level quantum chemistry calculations are required. However, the procedure can be simplified for polymers. The most important characteristics of polymer chain structure and chain mobility are governed by the backbone torsional motions. Therefore, one may expect that a force field which accurately describes the overall torsional potential of the backbone will correctly simulate the basic features of the polymer's structure and dynamics. Accuracy in the description of more detailed structural information and shorter time-scale motions such as vibrational frequencies may be sacrificed. However, these make negligible contributions to the overall chain structure and dynamics. In fact, many classical calculations were based on models with fixed bond lengths and bond angles. A simple procedure for developing a force field which provides correct backbone torsional potentials is described below.

The mechanical properties of polymers, particularly the stiffness matrix, have proved to be interesting topics for simulation studies.[2–5] This type of simulation has been encouraged by the fact that the calculated results often agree rather well with available experimental data. The calculation of mechanical properties requires one to evaluate the second derivatives of the potential energy with respect to the atomic coordinates (or displacement). This can be done analytically since the relationship between the potential energy and the coordinates is well-defined by the functional forms of the force field. However, when the system is very large, the analytical solution is not feasible because the second derivative matrix (the Hessian) becomes too large (it is proportional to the number of atoms squared). Many model amorphous polymers fall into this category. For these large systems one must use the finite difference method to evaluate the second derivatives. A detailed description of this approach was provided by Theodorou and Suter.[2] It was initially applied to systems with fixed density[2] and optimized density,[3] both systems using a cubic unit cell. Extending

* To whom correspondence should be addressed.

® Abstract published in *Advance ACS Abstracts*, March 15, 1994.

0024-9297/94/2227-2383$04.50/0

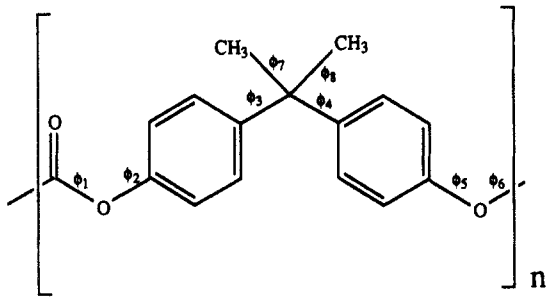

(a)

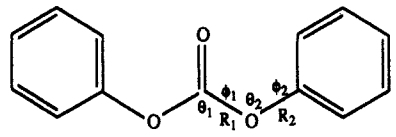

(b)

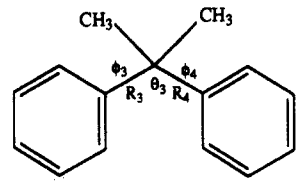

(c)

Figure 1. Structures of (a) Bisphenol A polycarbonate, (b) diphenyl carbonate (DPC), and (c) 2,2-diphenylpropane (DPP) and definitions of the geometric parameters used in the simulation.

the method to an orthorhombic unit cell is straightforward. However, the second derivative can only be evaluated correctly at a true local minimum where no constraint is applied. A full cell optimization is necessary where both the structure and the unit cell parameters are free to change. For amorphous polymers without any specific symmetry, this usually leads to a triclinic unit cell. A general approach for calculating the stiffness or compliance matrix of a triclinic unit cell is presented in the work reported here.

Optimizing the Force Field

As atomistic simulations of molecules and polymers attract more attention, the number of available force fields continues to increase. A carefully chosen force field may generate reasonable results. In some situations, one might be forced to develop a new force field. As mentioned previously, the effort involved must be weighed against the properties and phenomena one desires to simulate. In the case described here, a more realistic and utilitarian approach was taken, namely, to modify an existing force field, making it suitable for our purposes. This tactic was applied to polycarbonate using the repeat unit and the definition of dihedral angles as shown in Figure 1a. Four types of dihedrals are present: ϕ_1 is the same type as ϕ_6; the same relationship holds for ϕ_2 and ϕ_5, ϕ_3 and ϕ_4, and ϕ_7 and ϕ_8. The geometric parameters to be optimized in the modified force field are also defined in the Figure 1. The procedure includes (1) using a generic force field to calculate the torsional potential and local minima, (2) modifying a few parameters to fit the calculated results with quantum chemistry calculations, and (3) verifying the modified force field with available crystallographic and other structural data.

Molecular simulations were performed using POLYGRAF, a polymer simulation package from Molecular Simulations, Inc. The generic force field used was the Dreiding force field.[6] For an arbitrary geometry of molecules its potential energy, E, consists of the following terms:

$$E = E_B + E_A + E_T + E_I + E_{vdw} + E_Q \quad (1)$$

The first four terms are bonded energies: bond stretching (E_B), angle bending (E_A), torsion (E_T), and inversion (E_I). The last two terms are nonbonded energies: van der Waals interactions (E_{vdw}) and electrostatic interactions (E_Q). The Dreiding force field provides several functional forms for each of the energy terms. For example, for bond stretching, the harmonic function or the Morse function may be used. Similarly, for van der Waals interactions, either the Lennard Jones 12–6 or the exponential-6 functions may be employed. The definitions of each term used in this study are given in eqs 2–6.

$$E_B = \frac{1}{2}k_e(R - R_e)^2 \quad (2)$$

$$E_A = \frac{1}{2}K(\theta - \theta_0)^2 \quad (3)$$

$$E_T = \frac{1}{2}V\{1 - \cos[n(\varphi - \varphi_0)]\} \quad (4)$$

$$E_I = \frac{1}{2}K_{inv}(\Psi - \Psi_0)^2 \quad (5)$$

$$E_{vdw} = D_0\left\{\left[\left(\frac{6}{\zeta - 6}\right)\exp^{\zeta(1-(R/R_0))}\right] - \left[\left(\frac{\zeta}{\zeta - 6}\right)\left(\frac{R_0}{R}\right)^6\right]\right\} \quad (6)$$

The van der Waals interaction is exponential-6, *i.e.*, $E_{vdw} = Ae^{-CR} - BR^{-6}$. It is expressed in the form of eq 6 (with parameters D_0, R, R_0) so that it can be easily compared with the Lennard-Jones 12–6 form, where $E_{vdw} = D_0[(R/R_0)^{-12} - 2(R/R_0)^{-6}]$. ζ is a scaling factor. All the parameters in eqs 2–6 can be found in the Dreiding paper.[6] Partial atomic charges are neglected in this calculation ($E_Q = 0$).

Diphenyl carbonate (DPC) and 2,2-diphenylpropane (DPP) are used as model molecules for the polymer in the force field optimization. Their structures are shown in parts b and c of Figure 1, respectively, along with the definition of the parameters to be modified. The basic procedure used to optimize the force field can be illustrated by using backbone rotations ϕ_3 and ϕ_4 as an example. Details of this method will be described elsewhere.[7] We used the 2D energy contour plot (STO-3G level calculation)[8] of these two dihedral rotations of DPP as a reference. The goal is to fit the calculation of the modified force field to the plot in the reference. Only a single curve is needed for the fitting process: E vs ϕ with $\phi = \phi_3 = \phi_4 = 0, 5, 10, 15, ..., 90$. The 2D contour plot generated from the force field by fitting this single curve always agrees with the targeted 2D plot. This procedure not only makes the process simpler and more efficient but also greatly reduces the amount of data required from quantum chemistry calculations. In order to maintain the simplicity of the Dreiding force field, only three parameters related to the pair of rotations were changed: the equilibrium bond length (R_e in eq 2), the equilibrium bond angle (θ_0 in eq

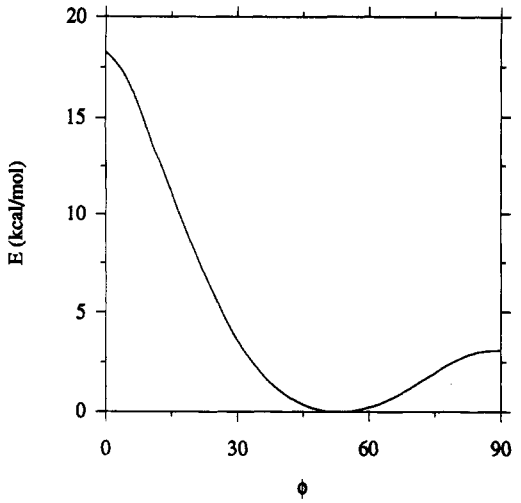

Figure 2. Potential energy (for $\phi_3 = \phi_4$) curve generated from the modified force field.

Table 1. Comparison between Modified Dreiding and *ab Initio* Calculations

	modified Dreiding	*ab initio*
ϕ_{min} (°) (ϕ_3 and ϕ_4)	53	~51
barrier at 0° (kcal/mol)	18.3	~17.5
barrier at 90° (kcal/mol)	3.13	~3.25

Table 2. Modified Dreiding Force Field Parameters for Polycarbonate

	modified	original
R_1 (Å)	1.3239	1.3200
R_2	1.4085	1.3500
R_3	1.4950	1.4600
$R(C_{arom}-H)$	1.0860	1.0200
θ_1 (deg)	104.00	120.00
θ_2 (deg)	114.00	104.51
θ_3 (deg)	109.00	109.47
V_1 (kcal/mol)	12.0	2.00
V_2 (kcal/mol)	3.60	2.00
V_3 (kcal/mol)	0.18	1.00

3), and the intrinsic torsional barrier (V in eq 4). The parameters which required fitting were the position of the minimum and the energy barriers at the two maxima (0° and 90°). This further reduced the requirements from quantum chemistry calculations. The final curve (E vs ϕ) from the modified force field is shown in Figure 2. Table 1 compares the three quantities with the *ab initio* calculations. Another criterion of the fitting process is that the final optimum geometry of the model structure be close to the experimental data or quantum chemistry data. The force field parameters related to rotation around ϕ_1 and ϕ_2 (and ϕ_6 and ϕ_5) were optimized with the same method using DPC as the model compound. The modified parameter values are listed in Table 2 along with the original Dreiding ones.

Since the *ab initio* calculations reveal the bond characteristics between atoms, the force field modification made according to the calculations can be partially explained by the chemical nature of the atoms involved, although the parameters themselves are merely the results of the optimization process. The most drastic change of the force field parameter is V_1. In the Dreiding force field the oxygen (in C–O–Ph), connecting the carbonate carbon and phenylene, can be either O_3 (sp^3) or O_R (resonant sp^2). In the former case $V_1 = V_2 = 2$ (kcal/mol), as listed in Table 2, and in the latter case $V_1 = V_2 = 25$ (kcal/mol). The modified force field distinguishes the two rotations (ϕ_1 and ϕ_2). The V_1 contains more contributions from the resonant double bond than V_2. The change in θ_2 also reflects hybridization changes. The angle is more open, showing the sp^2 characteristics.

The full 2D energy contour maps of all the torsions from the force field are plotted in Figure 3. The DPC is used in the calculation of parts a and b of Figure 3, and the DPP is used to obtain parts c and d of Figure 3. In each calculation the specified pair of dihedrals is constrained at certain desired values and the rest of the structure is allowed to move freely to minimize energy. These results generally agree with earlier works cited in ref 1. As shown in Figure 3a the carbonate group can only have a trans–trans or trans–cis conformation. The cis–cis conformation is prohibited. The energy of the trans–trans conformer is about 1.7 kcal/mol lower than that of the trans–cis conformer. The barrier between these two minima is about 8.8 kcal/mol. This group can therefore be considered fairly rigid. The interdependence of ϕ_2 and ϕ_1 is shown in Figure 3b. The local minima are located near $\phi_2 = \pm 70°$ or $\pm 110°$, while $\phi_1 = \pm 180°$. When ϕ_1 is confined to these values, the rotation of ϕ_2 becomes very easy. With a barrier of less than 1.5 kcal/mol, it varies over all values. The energy of local minima near $\phi_2 = \pm 90°$ and $\phi_1 = 0°$ is higher than those with $\phi_1 = \pm 180°$. These differences reflect the energy difference between trans–trans and trans–cis conformations of the carbonate group. Therefore, the local minima near $\phi_1 = 0°$ will be less populated than the ones where ϕ_1 is near $\pm 180°$. The two types of synchronous motion of ϕ_3 and ϕ_4 are clearly demonstrated in Figure 3c. In the one case, ϕ_3 and ϕ_4 increase or decrease simultaneously with a barrier of about 2.9 kcal/mol. In the other case, one dihedral increases while another decreases with a barrier of about 2.3 kcal/mol. (Both types of motion will be seen in the molecular dynamics study.) The interdependence of two side group rotations (ϕ_7 and ϕ_8) is shown in Figure 3d. Their rotations are also dependent on the two backbone dihedrals (ϕ_3 and ϕ_4). In the calculation of Figure 3d ϕ_3 and ϕ_4 are optimized. Therefore, the pattern of methyl rotation shown in the figure occurs only when the backbone dihedrals (ϕ_3 and ϕ_4) near their favorable conformations (see Figure 3c). The barrier (5.5 kcal/mol) is relatively high compared to the rotatable dihedrals on the backbone. The methyl rotation is severely hindered at lower temperatures as we will see later in the molecular dynamics study. The plots shown in Figure 3 are useful in analyzing the conformations, mobilities, and transition paths of different moieties of the polymer. They can also be used to develop statistical weight matrices for calculating rotational isometric states (RIS) and generating model polymer chains.

The agreement between the optimal geometries obtained from simulations of the model structure and the experimental or *ab initio* geometries of the same isolated molecular may not be sufficient to demonstrate the reliability of the modified force field although it is an important criterion. An important step is to compare the crystal structure predicted by the force field with the experimental data; thus the correctness of chain packing and long-range interactions can be verified. Since polycarbonate is almost completely amorphous (some incomplete earlier crystal data are available[9,10]), the crystal structure of a model compound, 4,4′-isopropylidenediphenylbis(phenyl carbonate),[11] was compared instead (see Figure 4). This model compound is a complete structural analogue of polycarbonate, demonstrating all its basic structural features. The model structure was built from experimental data, and a full optimization of atomic coordinates and cell parameters was performed afterward.

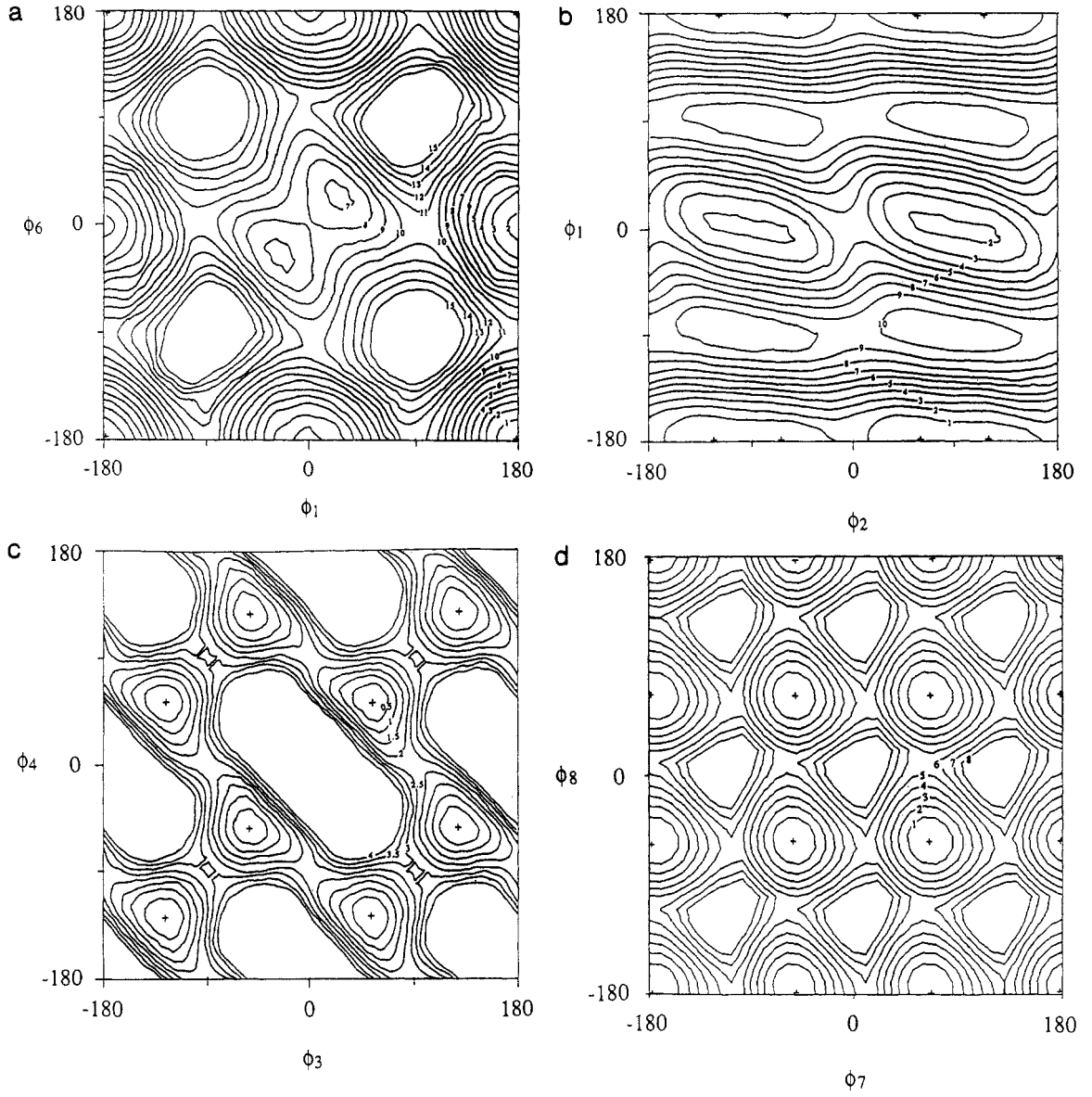

Figure 3. Conformational energy contours from the modified force field. Local minima are shown at +, and the unit for isoenergy lines is kcal/mol. (a) ϕ_1 vs ϕ_6; (b) ϕ_2 vs ϕ_1; (c) ϕ_3 vs ϕ_4; (d) ϕ_7 vs ϕ_8.

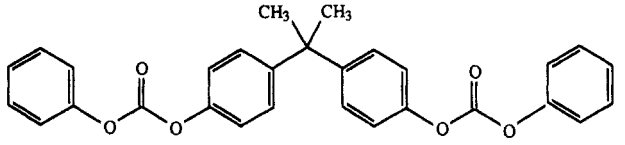

Figure 4. Schematic drawing of a model compound for polycarbonate, 4,4′-isopropylidenediphenylbis(phenyl carbonate).

Table 3. Experimental and Simulated Crystal Data for 4,4′-Isopropylidenediphenylbis(phenyl carbonate)

	exptl[11]	simulated
a(Å)	18.863	18.791
b (Å)	6.385	6.328
c(Å)	10.556	10.641
α (deg)	90.00	90.04
β (deg)	110.63	109.52
γ (deg)	90.00	89.93
V (Å^3)	1189.8	1192.7
d (g/cm^3)	1.31	1.305
space group	$P2_1$	$P2_1$

The Ewald summation technique was used for calculating nonbonded interactions. Table 3 lists the experimental and simulated crystal data. The root-mean-square (rms) difference between the atomic positions (without hydrogen) of two structures is 0.35 Å. The agreement is reasonably good. The simulated crystal structures projected on the *ac* and *bc* planes are shown in Figure 5. The optimized force field correctly describes the most important characteristics and interactions of the polycarbonate.

Model Structure of Amorphous Polycarbonate

The all-atom model of amorphous polycarbonate used in this study contained 691 atoms and had a degree of polymerization of 21. Periodic boundary conditions were adopted to simulate the condensed state. Six structures were built and optimized using multiple cycles of energy minimization and molecular dynamics as described previously.[12] Since the building of bulk polymers could be very time consuming, the building scheme used was chosen so that the final structures would be built as correctly as possible within a reasonable time frame. Two factors affecting the building process were considered: the distribution of the backbone dihedral angles and the initial density.

Backbone Dihedral Distributions. Normally the rotational isomeric states (RIS) model and the Monte Carlo method are combined to build an amorphous polymer chain. The states described by the RIS model can be defined using 2D energy contour maps as shown in Figure 3. Although one can build an isolated chain of polycar-

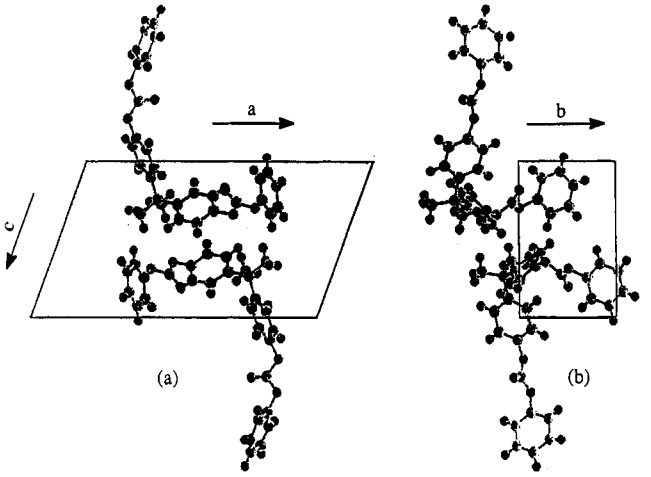

Figure 5. Simulated crystal structure of 4,4′-isopropylidenediphenylbis(phenyl carbonate): (a) in the *ac* plane; (b) in the *bc* plane.

bonate exhibiting these states relatively quickly, building bulk polycarbonate can be very slow if only the RIS states are allowed. The effectiveness of the process can be enhanced if more states are allowed or tolerance angles for each state are increased. The RIS model is most useful in generating energetically favorable polymer chains if no further optimization of coordinates follows. However, we used a minimization algorithm which resulted in a proper distribution of backbone dihedrals (the dihedrals distributed near the local minima on the potential energy surface as defined by the force field) even though the initial values were assigned randomly. The random assignment of backbone dihedrals can be interpreted for having the RIS continuous or extending the tolerance angle to 2π.

Figure 6 shows the distributions for dihedrals ϕ_3 and ϕ_4 for six model structures of polycarbonate as initially generated and following structural optimization. The initial distribution covers the entire conformational space uniformly (−180° to +180°) with many dihedrals in high-energy states. However, the distribution following optimization locates near the local minima noted previously on the contour map (Figure 3c). This final distribution is very similar to what would be expected from a proper RIS model. Most of the values for dihedrals ϕ_3 and ϕ_4 are within the 3 kcal/mol isoenergy line on the 2D contour plot, indicating that the optimization process is very effective. However, two pairs of dihedrals are trapped in relatively higher energy states (>4 kcal/mol). This may be attributed to the fact that it is more difficult for dihedrals to reach a local minimum in a densely packed structure since their ability to move is strongly dependent on the surrounding environment. More extensive annealing may therefore be necessary to eliminate these relatively bad conformations. Structural and conformational optimizations are much easier when building isolated chains.

Chain Packing and Relaxation. The effect of the initial density on chain packing was examined by building a total of six structures: two with initial densities of 1.0 g/cm^3, two with 1.2 g/cm^3, and two with 1.4 g/cm^3. Ideally, the densities of the final structures should match experimental values and be independent of their initial densities. The overall chain conformation of each structure may be quite different because of the random procedure used to assign backbone dihedrals. However, an effective structural optimization should produce final structures with similar energies and densities. The initial and final densities and energies for six model polycarbonate structures are listed in Table 4. The initial density specifies how densely the chain should be packed. It is evident that it will affect the final structure. The results shown in Table 4 suggest that the optimal initial density is a value (1.20 g/cm^3) slightly higher than the average final density (~1.15 g/cm^3). A higher value (1.40 g/cm^3) makes the packing process more difficult but shows no obvious improvement in the final structures. The energies are also higher. Forcing the chain to pack so densely may cause certain local conformations to be trapped in high-energy states which cannot be completely eliminated during structural optimization. When a lower initial density was used (1.00 g/cm^3), the building process was easier, but the resultant energies were somewhat higher and the final density never reached the values of those structures which started with higher initial densities. Perhaps certain favorable interactions which occur with denser packing are excluded. Apparently, the cell opti-

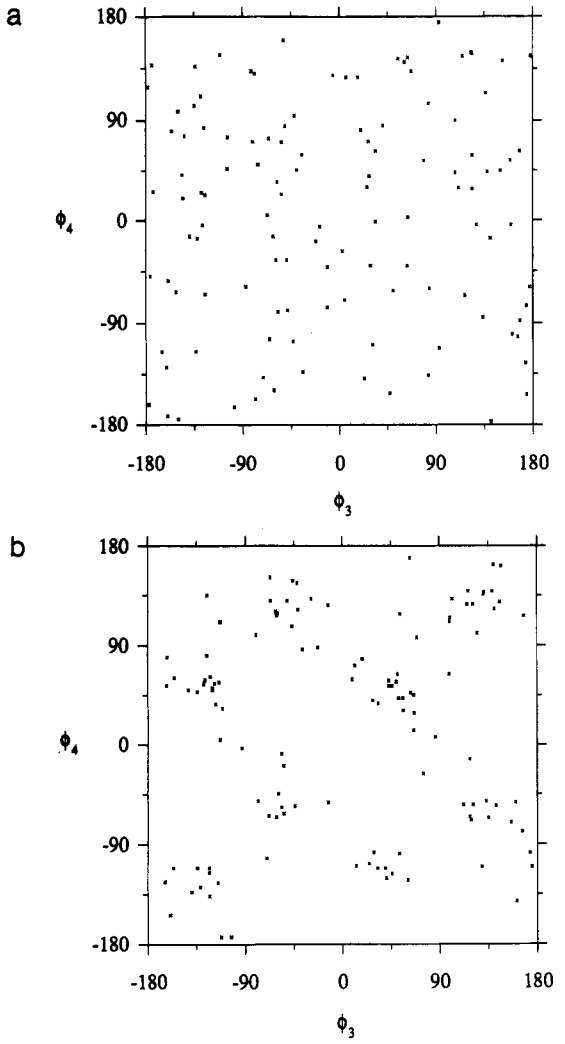

Figure 6. Dihedral angle distribution for pair ϕ_3 and ϕ_4 of six model polycarbonate structures: (a) as generated; (b) after structural optimizations.

Table 4. Initial Densities, Final Densities, and Energies of Six Model Polycarbonate Structures

structure	D_{int} (g/cm^3)	D_{fin} (g/cm^3)	E (kcal/mol)
1	1.4	1.169	443.51
2	1.4	1.194	443.25
3	1.2	1.175	426.73
4	1.2	1.181	416.59
5	1.0	1.074	436.07
6	1.0	1.075	436.98
ave		1.145	433.86
σ		0.055	10.44

Table 5. Average Internal Stress Components (MPa) of Six Model Polycarbonate Structures

xx	0.33 ● 0.32	yz	0.07 ± 0.48
yy	0.77 ± 0.75	zx	−0.13 ± 0.55
zz	0.47 ± 0.28	xy	−0.37 ± 0.50

mization process is capable of diffusing repulsive forces if the initial density is too high, even though all the bad contacts may not be eliminated. However, it does not appear to be able to overcome certain barriers required to form denser packing. Once the structures were built, there was little improvement in the density even though large external forces (stress or strain) were applied. The structures responded to the external force elastically; *i.e.*, the density returned to the value of the stress-free state when the external force was removed.

If the two structures with the lowest initial density (1.00 g/cm^3) are excluded, the average final density is 1.180 ± 0.011 g/cm^3, very close to the density of polycarbonate near room temperature, 1.20 g/cm^3.[13] However, energy minimization assumes the elimination of thermal motion. The densities of the simulated structures are therefore more properly compared to the experimental density at 0 K. Estimations from the density at room temperature and the volume thermal expansion coefficient of polycarbonate ($\sim 2.02 \times 10^{-4}$) give a value of 1.27 g/cm^3 at 0 K.[13] Our simulation value is about 7% lower. A similar error (5–6% lower) is observed for the model crystal structure of 4,4′-isopropylidenediphenylbis(phenyl carbonate) when its simulated density is compared to the estimated experimental value near 0 K.

In principle, this error could be traced from two sources, the force field and the packing scheme. Since no packing scheme (chain growth) is involved for the model crystal structure, one can conclude that the discrepancy is primarily due to the force field. It is reasonable to assume that the systematic error observed is due to the fact that the force field parameters were optimized against the crystal structures near room temperature rather than at 0 K. The packing scheme presumably accounts for the remaining 1–2% error found for the model amorphous structures. There may be some inherent difficulties in the procedure used to model chain growth in the condensed state or in the methods used to relax the structures after building them. Since the magic of polymer chain packing which occurs in nature is not fully understood, it is difficult to design a builder which simulates it completely.

The internal stress values obtained for our model structures indicate that the polymer chains are relaxed in the bulk glassy state. The internal stress components are defined as the first derivative of the potential energy with respect to displacement or strain. These values should be close to zero if the structure is located at a local minimum of the potential energy surface. If these components have large nonzero values, either positive or negative, the polymer chain is under either tension or compression. As shown in Table 5, the values for all the components of the internal stress tensor are small in magnitude, clearly indicating that the polymer chains are mechanically relaxed. This criteria usually cannot be satisfied if the density of the simulated structure is fixed. The average cell parameters for the six simulated structures are listed in Table 6. The deviations in cell lengths and angles are small even though full cell optimizations were performed (in addition to the coordinates, the shape of the cells were free to change).

Pair Distribution Functions and Structure Factor. The amorphous nature of the simulated structures can be demonstrated by calculating their pair distribution functions. One needs a complete set of pair distribution functions in order to fully characterize all the correlations between the different types of atoms. However, the dominating features of amorphous materials can be determined by just examining the total pair distribution function, $g(r)$. The $g(r)$ averaged from the six model structures is plotted vs distance (r) in Figure 7. No long-range order is seen. The peaks observed at distances less than 5 Å can be assigned to the specific distances of connected atoms (1–2, 1–3, and 1–4). This type of structural order due to intramolecular connections disappears at distances greater than 5 Å. Beyond this distance, the structures are completely randomized as far as the neighboring atomic positions are concerned. This is illustrated by the fact that our plot shows no visible peak at the well-defined distance (~5.76 Å) between the carbon and oxygen atoms in the segment C–Ph–O. Similar results have been observed in the aromatic polysulfone system.[12]

Table 6. Average Cell Parameters of Six Model Polycarbonate Structures

a (Å)	19.75 ± 0.39	α (deg)	91.43 ± 1.92
b (Å)	19.73 ± 0.28	β (deg)	90.63 ± 0.89
c (Å)	19.71 ± 0.51	γ (deg)	90.36 ± 1.62

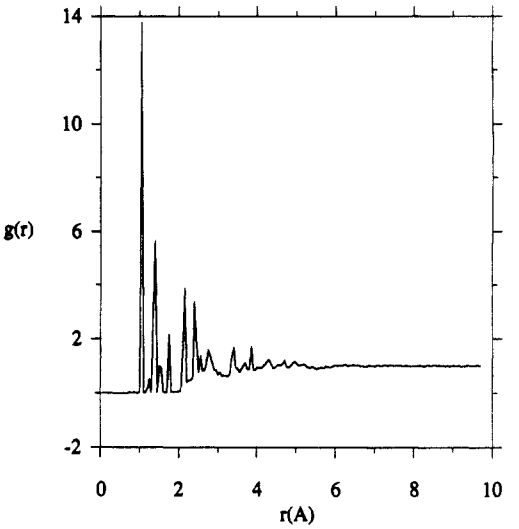

Figure 7. Total pair distribution function of model polycarbonate.

The averaged pair distribution function excluding H atoms of the same structures, $g(r)'$, is shown in Figure 8, where $g(r)' = g(r)_{C-C} + g(r)_{O-O} + g(r)_{C-O}$. Obviously the information contained in $g(r)'$ is included in $g(r)$. The structure factor is calculated from the pair distribution function through the following equation:[14]

$$S(k) = 1 + (4\pi\rho/k)\int_0^\infty dr \sin(kr)\, r[g(r) - 1] \qquad (7)$$

where k is the wave vector and ρ is the atom density. The $S(k)$ obtained from $g(r)'$ agrees better with experimentals[15] than $g(r)$, as shown in Figure 9. The observed experimental maxima appear at $k \sim 1.3$, 3.1, and 5.3 Å^{-1} with two shoulders near 0.7 and 1.8 Å^{-1}. Using $g(r)'$ means that scattering factors of C and O are weighted equally, while H's is neglected completely. This is a reasonable assumption since the scattering power of hydrogen is negligible compared to oxygen and carbon. The calculated $S(k)$ from eq 7 will not match the experimental intensity since the k dependence of the scattering factor is not considered. The agreement in peak positions between simulation and experiments demonstrates that the protocol used here for building an amorphous polymer by random generation of

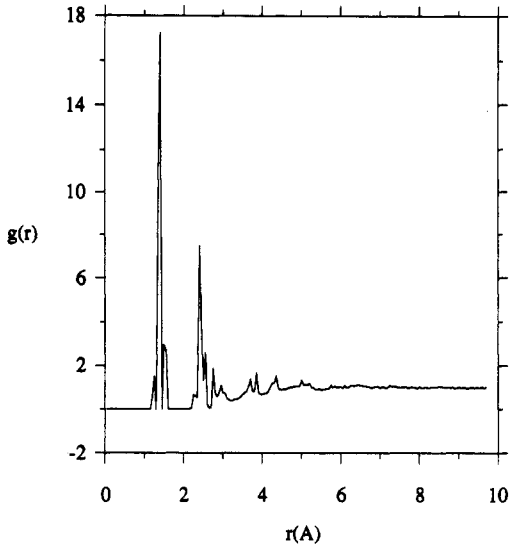

Figure 8. Pair distribution function excluding H atoms for the model structure of polycarbonate.

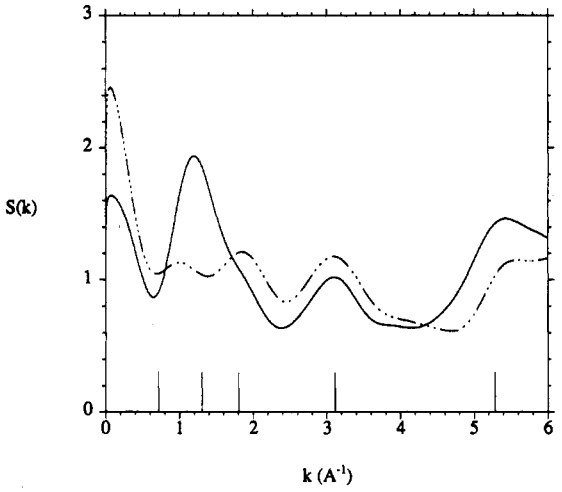

Figure 9. Structure factors of model polycarbonate calculated from the pair distribution functions $g(r)$ (dotted and dashed line), $g(r)'$ (solid line), and experimental peak position (vertical lines).

dihedrals, followed by extensive annealing and structural optimization, reliably produces model structures which are good representations of the real polymer.

Mechanical Properties

Molecular mechanics can be used to calculate either the compliance matrix by applying external stress or the stiffness matrix by applying external strain. The components of the stiffness matrix can be defined by

$$C_{ij} = \partial\sigma_i/\partial\epsilon_j \tag{8}$$

where σ_i and ϵ_j are stress and strain components, respectively ($i,j = 1, 2, ..., 6$). In the simulation each component of C_{ij} is calculated by measuring the response of stress σ_i when a very small strain ϵ_j is applied. The stiffness matrix calculation usually is very efficient. This is because the internal stresses are very sensitive to the dimension change and no full cell optimization is required. The fundamentals of the method have been discussed in an earlier work on polypropylene.[2] The main limitation of the original version is that it only applies to cubic and orthorhombic unit cells. For these systems the cell vectors a, b, and c coincide with Cartesian axes x, y, and z ($\alpha = \beta = \gamma = 90°$). There is a one-to-one relationship between the strain components and the cell parameters. Applying a desired external strain is straightforward: changing only one of six cell parameters.

The need for generalization of the method is obvious since full optimization of a structure may lead to a cell shape other than cubic and orthorhombic. For a system like this one may not be able to apply a desired external strain by simply changing one of the cell parameters. For example, in a triclinic system applying a strain in the x direction (ϵ_1) requires changing not only a but also b, c, α, β, and γ. A more general method therefore should consist of the following steps. For each external strain component (ϵ_j) a new set of cell parameters should be calculated. Then one should apply the new cell parameters to the structure and optimize it while keeping the shape fixed. The component C_{ij} of the stiffness matrix is obtained from the change of stress component σ_i and applied strain ϵ_j. Here we present a scheme for such a calculation.

A unit cell with an arbitrary shape can be completely described by three cell vectors: **a**, **b**, and **c**. A 3×3 matrix **h**[16] is defined such that its columns are the components of **a**, **b**, and **c**:

$$\begin{pmatrix} \mathbf{a} \\ \mathbf{b} \\ \mathbf{c} \end{pmatrix} = \mathbf{h}^{\mathrm{T}} \begin{pmatrix} \mathbf{x} \\ \mathbf{y} \\ \mathbf{z} \end{pmatrix} \tag{9}$$

where $\mathbf{h}^{\mathrm{T}}$ is the transposition of **h** and **x**, **y**, and **z** are the three unit vectors of the Cartesian coordinate frame. If the cell axis is chosen so that **c** is parallel to the z axis and **b** is in the y–z plane, then the elements of **h** (or the components of **a**, **b**, and **c**) are given by

$$\mathbf{h} = \begin{pmatrix} a\sin\beta\sin\gamma^* & 0 & 0 \\ a\sin\beta\cos\gamma^* & b\sin\alpha & 0 \\ a\cos\beta & b\cos\alpha & c \end{pmatrix} \tag{10}$$

where a, b, c, α, β, and γ are the lengths and angles of the cell and $\cos\gamma^* = (\cos\gamma - \cos\alpha\cos\beta)/(\sin\alpha\sin\beta)$. A matrix **G** is defined as the product of **h** and its transposition $\mathbf{h}^{\mathrm{T}}$:

$$\mathbf{G} = \mathbf{h}^{\mathrm{T}}\mathbf{h} \tag{11}$$

The relationships between the strain tensor ϵ, the reference cell shape $\mathbf{h}_0$ prior to deformation, and the new cell shape after deformation **h** (or **G**) are given by the following equation[17]

$$\epsilon = (\mathbf{h}_0^{\mathrm{T}-1}\mathbf{G}\mathbf{h}_0^{-1} - 1)/2 \tag{12}$$

where $\mathbf{h}_0^{\mathrm{T}-1}$ is the inverse of $\mathbf{h}_0^{\mathrm{T}}$ and $\mathbf{h}_0^{-1}$ is the inverse of $\mathbf{h}_0$. 1 is the identity matrix. Here the components of the strain tensor ϵ are double indexed. The relationship between double-indexed components (ϵ_{ij}, $i,j = 1, 2, 3$) and single-indexed components (ϵ_j, $j = 1, ..., 6$) is well-defined.[18]

In the stiffness matrix calculation the input information is strain and initial cell shape, i.e., ϵ and $\mathbf{h}_0$. The output is new cell shape (six cell parameters). By rearranging eq 12, the components of the **G** matrix can be obtained through

$$\mathbf{G} = \mathbf{h}_0^{\mathrm{T}}(2\epsilon + 1)\mathbf{h}_0 \tag{13}$$

Using eqs 10 and 11, one obtains a set of six independent equations, $G_{ij} = G_{ij}(a,b,c,\alpha,\beta,\gamma)$. Solving this set of equations leads to the following relationships between the

cell parameters and the components of the G matrix:

$$a = G_{11}^{1/2}$$

$$b = G_{22}^{1/2}$$

$$c = G_{33}^{1/2}$$

$$\cos\alpha = G_{32}/(G_{22}G_{33})^{1/2}$$

$$\cos\beta = G_{31}/(G_{11}G_{33})^{1/2}$$

$$\cos\gamma = G_{21}/(G_{11}G_{22})^{1/2} \quad (14)$$

By assigning these new cell parameters to the structure, the desired external strain is employed.

The calculation of stiffness matrix **C** therefore can be summarized in the following steps:

1. Optimize the cell parameters of the undeformed structure to obtain $\mathbf{h}_0$.
2. Calculate **G** using eq 13 and the cell parameters using eq 14 under the strain of ϵ_{j+}, a positive strain in the j direction.
3. Assign the new cell parameters to the system, optimize the structure with a fixed shape and obtain the internal stress tensor σ_+.
4. Repeat steps 2 and 3, applying ϵ_{j-}, a negative strain in the j direction, to obtain σ_-.
5. Calculate C_{ij} using the finite difference method, $C_{ij} = (\sigma_{i+} - \sigma_{i-})/(\epsilon_{j+} - \epsilon_{j-})$, $i = 1, 6$.
6. Repeat steps 2–5 with different j's, $j = 1, 6$.

The internal stress is very sensitive to the strain. One can therefore apply very small strain to perform the calculation. The stiffness matrix shows very little change for applied strains ranging from 1.0×10^{-5} to 1.0×10^{-3}. The minimization process in step 3 converges very quickly (rms force 0.1 kcal/mol/Å). The computing time required to calculate the stiffness matrix can be 1 or 2 orders of magnitude less than that required to calculate the compliance matrix. The calculated stiffness matrix averaged for six model polycarbonate structures is shown in eq 15 (in GPa). The applied strain is 0.01% (1.0×10^{-4}).

$$\mathbf{C} = \begin{pmatrix} 6.69 & 2.52 & 2.01 & -0.07 & -0.30 & -0.11 \\ 2.29 & 5.88 & 2.30 & -0.02 & 0.04 & -0.41 \\ 2.21 & 1.62 & 6.57 & -0.09 & -0.17 & 0.42 \\ 0.21 & 0.06 & -0.05 & 2.12 & 0.33 & 0.05 \\ -0.30 & 0.04 & 0.09 & 0.43 & 1.70 & -0.11 \\ 0.17 & -0.89 & 0.45 & -0.02 & -0.10 & 2.25 \end{pmatrix} \quad (15)$$

At the macroscopic level, the strain energy of materials is a function of only the state of the body; therefore, the stiffness matrix should always be symmetric, i.e., $C_{ij} = C_{ji}$.[19] However, in our computations, the C_{ij} and C_{ji} are obtained using different finite deformation paths as discussed above. In the energy minimization process after the deformation, the structure settles in one of many similar local minima, not a unique global minimum. Therefore, the microscopic nature of the model polymer, the finite deformation process, and the limitation in the energy minimization make the strain energy depend on the followed deformation path, although very weakly, and thus this leads to the nonsymmetric feature of the calculated stiffness matrix. The averaged stiffness matrix shows the basic features of an isotropic material. The values of the diagonal terms in the three principle directions are similar, as are the three shear moduli. The terms which would be expected to be zero for an ideal isotropic material are much smaller than the nonzero terms. The Young's modulus, shear modulus, bulk modulus, the Poisson's ratio derived from the stiffness matrix are listed in Table 7. The calculated values are about twice as high as those obtained experimentally (5.03 vs 2.34 GPa for the Young's modulus, and 2.02 vs 0.78 GPa for the shear modulus).[13] As discussed before, one reason for this discrepancy is that the simulated system represents ideal structures, whereas the experimental sample may contain many microscopic or even macroscopic defects. The applied strain (stress) which was used for the experimental testing method was also much larger than that used in the simulations. One would therefore expect molecular simulations to yield higher values. If the moduli of amorphous polymers could be measured by a technique similar to what X-ray scattering has done for measuring moduli of crystalline polymers, the simulated results would have been much closer to experimental values. The temperature difference between simulation (0 K) and experiment (room temperature) may also play a role. More reasonable results could be obtained using molecular dynamics simulations at room temperature where thermal softening is automatically taken into account.[4] Another source of error may be that the force field is optimized only for the torsional potentials not the vibrational spectrum. However, this probably has little effect. In general, the mechanical constants obtained from simulations provide the upper limit of the polymer and should serve this purpose in designing new compounds. The higher values in Young's modulus and the shear modulus of polycarbonate were also reported by Hutnik et al.[20]

Table 7. Average Mechanical Constants of Six Model Polycarbonate Structures

Young's modulus (GPa)	5.03 ± 0.81
shear modulus (GPa)	2.02 ± 0.47
bulk modulus (GPa)	3.68 ± 0.74
Poisson's ratio	0.24 ± 0.09

Molecular simulations were also used to study the deformation behavior of the model polymers. Uniaxial tensile strain was applied in the z-direction by changing cell length c. The z axis is coincident with the c axis, making it easy to determine the new c value for each applied strain. Since there is no inherent anisotropy for the structures, this choice should make little difference for the final results. In the structural optimization of each strain step (0.2%) the cell parameters other than c were allowed to vary. The maximum engineering strain applied was about 15%. The stress–strain curve for each individual structure can be very variable. The averaged one should reduce the noise caused by the fluctuations from structure to structure and should reveal the more fundamental nature of the deformation behavior of the model polymer. Figure 10 shows the averaged stress–strain curve (σ_3 vs ϵ_3). The volume of model structures increases during stretching, initially fast and then reaching a steady Poisson's value of about 0.31. It is clear that the yield phenomenon is observed in the simulation. The yield stress (~0.25 GPa) is much higher than the experimental value (0.062 GPa); the elongation at yield (~10%) compares favorably with the experimental values (6–8%).[13]

Conclusions

The simple force field optimization method used in this study, based on a generic force field and *ab initio* calculations, generates a set of good force field parameters for the torsional potential of the model polycarbonate. Simulations performed using this modified force field reproduced the crystal structure of a model compound for

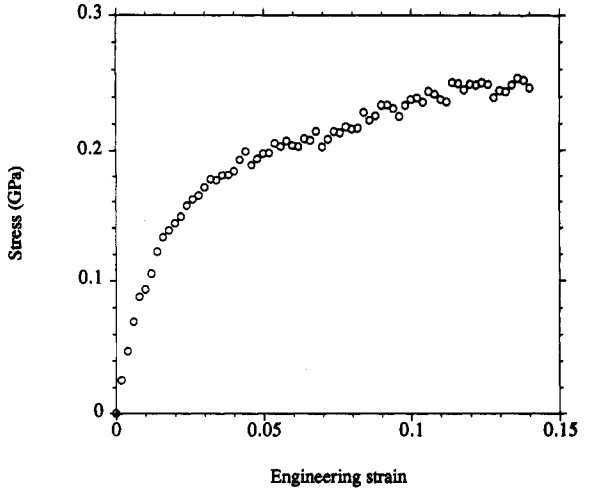

Figure 10. Averaged stress–strain curve of model polycarbonate.

the polymer. The initial density assigned in the building process affected chain packing. Lower final densities were obtained for structures which started with the lowest initial density. The structure factor calculated for the model polymer agreed well with X-ray scattering data, indicating that the model is a good representation of the experimental structure. A general method for calculating the mechanical properties (stiffness matrix) of any shape unit cell was presented. The calculated mechanical constants were generally higher than the experimental values. This is probably due to the differences between the simulated system which represents ideal structures and the real sample which may contain defects. The temperatures used were also different. The yield phenomenon was observed at large deformation. The yield stress was higher than experimental values; the yield strain was close to the experimental one.

Acknowledgment. We thank Dr. Marie Ary for her contribution in this work.

References and Notes

(1) Hutnik, M.; Argon, A. S.; Suter, U. W. *Macromolecules* **1991**, *24*, 5956, 5970. Hutnik, M.; Gentile, F. T.; Ludovice, P. J.; Suter, U. W.; Argon, A. S. *Macromolecules* **1991**, *24*, 5962.
(2) Theodorou, D. N.; Suter, U. W. *Macromolecules* **1986**, *19*, 139.
(3) Fan, C. F.; Hsu, S. L. *Macromolecules* **1992**, *25*, 266.
(4) Cagin, T.; Karasawa, N.; Dasgupta, S.; Goddard, W. A. *MRS Symp. Proc.* **1992**, *278*, 61.
(5) Karasawa, N.; Goddard, W. A. *Macromolecules* **1992**, *25*, 7268.
(6) Mayo, S. L.; Olafson, B. D.; Goddard, W. A. *J. Phys. Chem.* **1990**, *94*, 8897.
(7) Fan, C. F.; Goddard, W. A., in preparation.
(8) Laskowski, B. C.; Yoon, D. Y.; McLean, D.; Jaffe, R. L. *Macromolecules* **1988**, *21*, 1629.
(9) Prietschk, A. *Kolloid Z.* **1958**, *156*, 8.
(10) Bonart, R. *Makromol. Chem.* **1966**, *92*, 149.
(11) Perez, S.; Scaringe, R. P. *Macromolecules* **1987**, *20*, 68.
(12) Fan, C. F.; Hsu, S. L. *Macromolecules* **1991**, *24*, 6244.
(13) Margolis, J. *Engineering Thermoplastics*; Marcel Dekker: New York, 1985.
(14) Chandler, D. *Introduction to Modern Statistical Mechanics*; Oxford University Press: New York, 1987.
(15) Neki, K.; Geil, P. H. *J. Macromol. Sci.* **1973**, *B8*, 295. Saffell, J. R.; Windle, A. H. *J. Polym. Sci., Polym. Lett.* **1980**, *18*, 377. Mitchell, G. R.; Windle, A. H. *Colloid Polym. Sci.* **1985**, *263*, 280.
(16) Parrinello, M.; Rahman, A. *J. Appl. Phys.* **1981**, *52*, 7182.
(17) Ray, J. R. *Comput. Phys. Rep.* **1988**, *8*, 109.
(18) Mase, G. E. *Continuum Mechanics*; McGraw-Hill: New York, 1970.
(19) Nye, J. F. *Physical Properties of Crystals*; Clarendon Press: Oxford, U.K., 1985.
(20) Hutnik, M.; Argon, A. S.; Suter, U. W. *Macromolecules* **1993**, *26*, 1097.